






## Article

# Distributed Optical Fiber-Based Radiation Detection Using an Ultra-Low-Loss Optical Fiber

Luca Weninger <sup>1,\*</sup>, Adriana Morana <sup>1</sup>, Youcef Ouerdane <sup>1</sup>, Emmanuel Marin <sup>1</sup>, Aziz Boukenter <sup>1</sup>  
and Sylvain Girard <sup>1,2,\*</sup>

<sup>1</sup> Laboratoire Hubert Curien, UMR-CNRS 5516, Université Jean Monnet, 42000 Saint-Etienne, France; adriana.morana@univ-st-etienne.fr (A.M.); youcef.ouerdane@univ-st-etienne.fr (Y.O.); emmanuel.marin@univ-st-etienne.fr (E.M.); aziz.boukenter@univ-st-etienne.fr (A.B.)

<sup>2</sup> Institut Universitaire de France (IUF), Ministère de l'Enseignement Supérieur et de la Recherche, 75005 Paris, France

\* Correspondence: luca.weninger@univ-st-etienne.fr (L.W.); sylvain.girard@univ-st-etienne.fr (S.G.)

**Simple Summary:** Distributed optical fiber sensors based on reflectometry techniques are showing great promise to monitor the evolution of different environmental parameters along one optical fiber. Among these, the design of a fiber-based distributed radiation detector can be a very powerful tool for large radiation facilities and accelerators. We conceive such a sensor by combining optical time domain reflectometry and a radiation-sensitive ultra-low-loss optical fiber that presents very high infrared radiation-induced attenuation as soon as it is exposed to radiation while quickly recovering after the end of exposure. We characterize the performances of this sensor technology: its radiation detection capability, its spatial resolution, and its capacity to quantify the radiation field (dose, dose rate) as a function of various fiber pre-irradiation treatments.

**Abstract:** The combination of an ultra-low-loss optical fiber sensitive to ionizing radiation and an optical time domain reflectometer (OTDR) is investigated to explore the feasibility of a single-ended distributed radiation detector. The peculiarity of the tested fiber resides in its regenerative high radiation-induced attenuation (RIA) response in the infrared spectrum (1310 nm), which returns to a low value once the irradiation has ended, combined to its sensitivity, highly increasing with the dose rate. In this work, only some sections of the fiber line were irradiated with 100 kV X-rays at room temperature, to prove the spatially resolved radiation detection capabilities of the system. The transient RIA response of the fiber was characterized at different pre-irradiation doses. A pre-irradiation treatment was shown to stabilize the optical fiber response, improving its RIA vs. dose rate linearity and repeatability. This improved response, in terms of radiation quantification, comes at the cost of a lower detection threshold. This work lays the bases for a distributed radiation detector, with some capabilities in dose rate evaluation.

**Keywords:** radiation detection; optical fibers; ionizing radiation; OTDR; distributed sensing



**Citation:** Weninger, L.; Morana, A.; Ouerdane, Y.; Marin, E.; Boukenter, A.; Girard, S. Distributed Optical Fiber-Based Radiation Detection Using an Ultra-Low-Loss Optical Fiber. *Radiation* **2024**, *4*, 167–182. <https://doi.org/10.3390/radiation4020013>

Academic Editor: Jean Paul Jay-Gerin

Received: 21 April 2024

Revised: 17 May 2024

Accepted: 28 May 2024

Published: 30 May 2024



**Copyright:** © 2024 by the authors. Licensee MDPI, Basel, Switzerland. This article is an open access article distributed under the terms and conditions of the Creative Commons Attribution (CC BY) license (<https://creativecommons.org/licenses/by/4.0/>).

## 1. Introduction

There are many technologies that would benefit from the implementation of optical fiber-based distributed radiation detectors: from irradiation beam lines that could be monitored through a single optical fiber, instead of multiple point detectors, to space vessels that could be constantly monitored throughout the whole volume of the spacecraft. Radiation detectors should be able to identify the presence of radiation quickly and reliably, but also to resist the cumulative dose effects without losing their detection performance.

### 1.1. Optical Time Domain Reflectometry Dosimetry

As shown in [1–6], the combination of reflectometry techniques with radiation-sensitive phosphosilicate (P-doped) optical fibers (OFs) can introduce a solution capable of detecting

and quantifying radiation throughout the whole length of an OF with a single-ended instrument, like an optical time domain reflectometer (OTDR) [7]. An OTDR is a single-ended distributed fiber sensing technique largely employed in telecommunication systems for fiber diagnostics. It employs a time-of-flight technique based on Rayleigh scattering to measure the attenuation along an optical fiber. A short light pulse is sent along the fiber. While traveling inside it, this pulse interacts with its glass matrix, which results, among others, in a back-scattered Rayleigh signal at the same wavelength of the probe signal. This signal will return toward the instrument, which will acquire its intensity as a function of time. Knowing the speed of light inside the fiber, the intensity measured by the detector at each instant can be associated with the position along the fiber from where the back-scattered signal comes from. As a result, by comparing the injected signal and the backscattered signal, it is possible to estimate the optical losses relative to a certain point of the OF. In its most simple configuration, the input pulse duration is the key factor in determining the spatial resolution achievable with this technique [8]. With modern OTDRs working in the infrared spectrum at telecommunication wavelengths, the spatial resolution is around 50 cm, using a pulse duration around 5 ns [2,9]. As an example, this technique is usually employed over several tens of km of optical fiber to precisely individuate the position of any breaks or bending losses that are present along the telecom line. The aforementioned distributed dosimeters are based on the most impacting phenomenon happening to an OF under ionizing radiation, called radiation-induced attenuation (RIA) [10,11]. When an OF is exposed to ionizing radiation, this will interact with its glass matrix, generate defects, or convert precursor sites into optically-active centers that will affect the propagating signal, absorbing it [12,13]. The structure and the optical properties in terms of absorption bands of these defects depend on the fiber chemical composition, on the mechanical properties of the fiber (dimensions, shape, drawing process, etc.), and on the external conditions of irradiation (temperature, injected power, etc.) [14]. The optical absorption bands related to the defects will absorb the light traveling through the fiber and increase its total attenuation. The RIA is the quantification of these excess losses introduced under ionizing radiation. The main parameter driving the response of an OF is the core and cladding glass composition selected to design the refractive index profile.

### *1.2. Choosing an Optical Fiber*

Depending on the materials, the OF can either be classified as radiation hard (or resistant), which is the case for F-doped and pure-silica core (PSC) OFs for most of the steady-state radiation environments, or radiation sensitive, like in the case of Al- or P-doped OFs [12,15]. P-doped fibers have been extensively investigated and implemented in several radiation environments to be used as cumulative dose sensors thanks to their many excellent characteristics [3,16,17]. The RIA at 1550 nm of this optical fiber depends linearly on the total ionizing dose (TID), up to at least 500 Gy [1,17]. It was proven to be resistant to the influence of dose rate, between 1  $\mu\text{Gy/s}$  and 10 Gy/s [1,2,17], together with its weak recovery after irradiation. To give the reader an order of magnitude about these dose rate values, equipment sent to space missions generally encounters dose rates between a few  $\mu\text{Gy/s}$  to a few mGy/s, depending on the orbit and amount of shielding in place. Radiotherapy ranges from tens of mGy/s for long treatments up to hundreds of kGy/s in new FLASH therapy techniques. There are then high-energy physics applications, like the Large Hadron Collider at CERN, where the dose rates range between tens of mGy/s to a few Gy/s. It should then come as no surprise that this sensing solution has already been implemented as a distributed fiber radiation sensor in some applications. An example of application involving optical fibers is [3], where researchers instrumented an accelerator line at CERN with this OF to monitor the circumference of the beam line with a single fiber. These fibers have also been investigated under gamma and X-ray irradiations for a miniaturized system [2].

### 1.3. A Regenerating Detector: The Vascade Optical Fiber

While a cumulative dosimeter is useful in many applications, one important limitation lays in the maximum dose that can be observed, due to the difficulty in restoring the active element of the system (in this case, the OF) to its initial state. To obtain such a characteristic, the RIA should recover completely once the irradiation is over to permit the reuse of the fiber, as was proven in [18] for a P-doped OF. In this case though, a careful choice of light injection source is needed to obtain enough regeneration of the fiber transmission. Recently, multiple publications have been devoted to the study of a particular ultra-low-loss PSC fiber (ULL-PSCF) [19–23]. The RIA response of this OF differs from most other PSC fibers, which are among the most radiation-resistant under steady-state radiation [24,25]. The RIA sensitivity in the infrared (IR) range of this OF can even be higher than the aforementioned P-doped fiber at high dose rates, and it recovers almost completely once the irradiation has ended. More in detail, it was shown that during irradiation, the RIA in the IR range is composed of a limited permanent contribution, which increases with dose and stabilizes at a certain level, and a huge transient contribution, which quickly reaches a maximum level depending on the dose rate and disappears once the irradiation is over [23]. This transient RIA is typical of a particular defect, known in the literature as self-trapped holes (STHs) [19,26–31]. As a first explanation, the radiation response of this ULL OF can be attributed to the advanced manufacturing process that has been used to achieve such ultra-low losses, down to  $\sim 0.16$  dB/km, at 1550 nm [19], very close to the Rayleigh theoretical limit in SiO<sub>2</sub> of 0.14 dB/km [32]. The details of this process are still unknown to this day, but it was confirmed to impact the fictive temperature of the silica glass inside the fiber, and this is known to affect the concentration of the STHs. Another important phenomenon that takes place in this fiber type is the photobleaching (PB) effect, meaning the light-induced annealing of optical absorbing defects: it has shown a strong decrease in the transient RIA levels at increasing signal power densities at both 1310 nm and 1550 nm. In [22], the authors report a decrease in RIA at 1310 nm up to 98% between injected powers of  $\sim 100$  nW and 1 mW. Interestingly enough, this effect does not seem to affect the permanent part of the IR-RIA. Recently, our group also proved that the fiber radiation response changes after X-ray pre-irradiation at 1 MGy [23]. Indeed, considering this first irradiation at 1 MGy as pre-treatment, hence calculating the RIA starting from the losses of the pre-irradiated fiber, greatly reduces the influence of the dose-dependent permanent losses. This leads to an ON–OFF RIA response jumping between almost zero and the transient RIA level, whose height depends on dose rate. Pre-irradiation was also shown to greatly reduce the switching time between the RIA levels in the presence or absence of irradiation, down to a 90%-to-10% recovery time of around 20 s. These characteristics sparked the idea of a possible RIA-based distributed radiation detector, an application domain heavily populated by radiation-induced emission (RIE) fiber-based solutions [33,34]. These are based on the light emission process generated by the relaxation of radiation-induced defects inside particularly doped optical fibers. Many studies have shown the promise of this approach for dose rate monitoring, optimizing the setup and the fiber of choice, but the solutions proposed today are not compatible with distributed measurements. As for the ULL-PSCF, the interesting wavelengths of the RIA response are focused in the IR spectrum; with the maximum of the optical absorption being around 1270 nm, it is then possible to pair this OF with all the reflectometry techniques that operate in the second and third telecommunication bands (at 1.31 and 1.55  $\mu\text{m}$ ) to build a distributed radiation detector. The effect of PB needs to be kept in mind, as these devices inject light signals in the order of 1 mW to map the fiber, and this can be the most limiting factor for more precise techniques, such as optical frequency domain reflectometry (OFDR), which would need to inject around 10 mW of power to map the losses along the fiber with a precision of a few centimeters [9,35]. The goal of this paper is then to investigate the compatibility of this ULL-PSCF with a commercially available OTDR system operating at 1310 nm, to obtain a single-ended sensor capable of detecting the distribution of ionizing radiation along the optical fiber. All the doses in this article are reported in Gy(SiO<sub>2</sub>).

## 2. Materials and Methods

### 2.1. Optical Fiber under Test

The investigated optical fiber is a ULL-PSC and F-doped cladding single-mode optical fiber, the Vascade EX1000 from Corning (New York, NY, USA) [36]. It has an attenuation of  $\sim 0.16$  dB/km at 1550 nm. The spectral response of this fiber together with the energy-dispersive X-ray (EDX) spectroscopy measurements of its chemical elements and their radial distribution were presented in [19]. Figure 1 reports the RIA kinetics at 1310 nm under a 5 min irradiation at 14 Gy/s, obtained with a classical spectral RIA measurement setup, the same as the one used in [23], composed of a white light source (few  $\mu$ W of injected power) on one side of the fiber under test and an IR spectrometer on the other side.

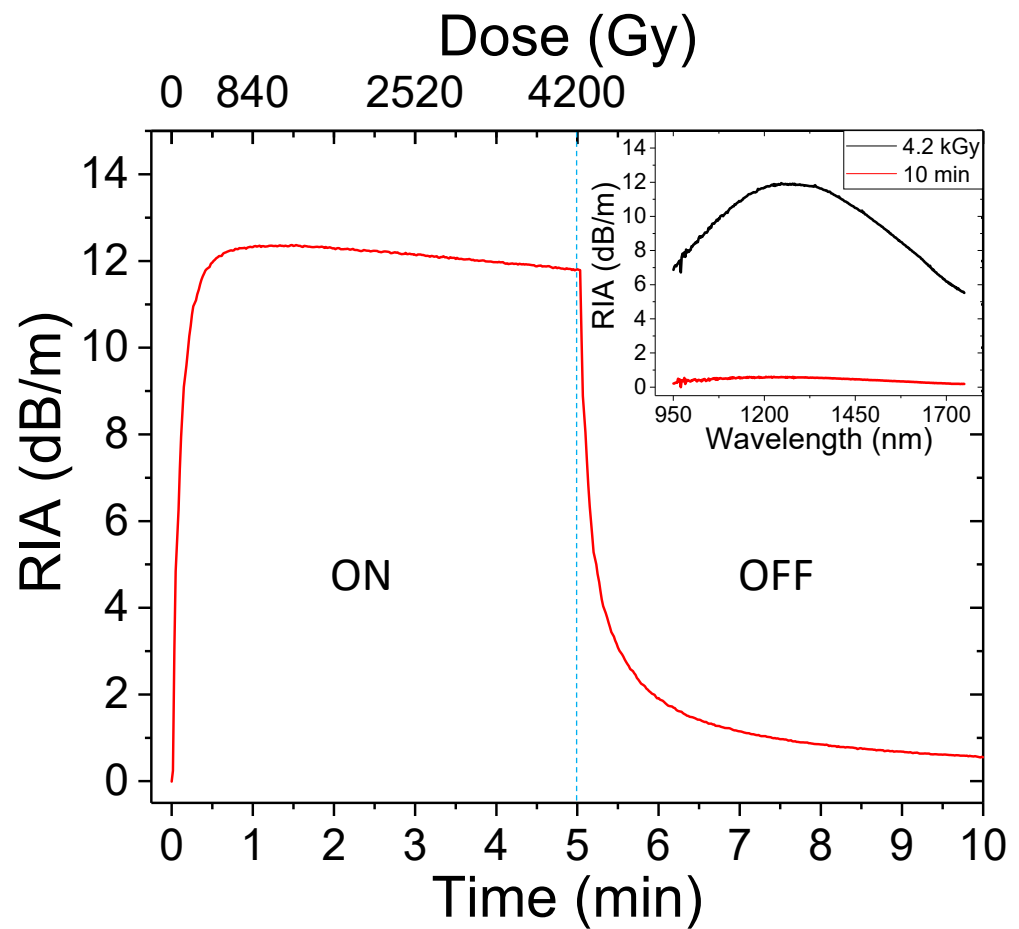


**Figure 1.** RIA kinetics at 1310 nm of the Vascade optical fiber during a 5 min irradiation at 14 Gy/s. The blue dashed line corresponds to the end of the irradiation period. The inset shows the spectral RIA response in the IR at the 5 min mark, at 4.2 kGy, and at the 10 min mark, after 5 min of recovery.

The reported kinetics describe how the RIA increases quickly during irradiation up to a maximum point around 12.3 dB/m, and then decreases toward a slightly lower value,  $\sim 11.8$  dB/m. Once the irradiation is over after 4.2 kGy, at the 5 min mark, the radiation-induced losses quickly return to a lower constant value,  $\sim 0.56$  dB/m, which corresponds to a recovery of about 95% after 5 min. This behavior is also observable in the inset of Figure 1, which reports the spectral RIA response in the infrared of the investigated fiber after 4.2 kGy at 14 Gy/s and at the 10 min mark, after 5 min of recovery.

### 2.2. Optical Time Domain Reflectometer in Use

The measurements presented in this work were obtained using the MTS 4000 V2 OTDR from Viavi Solutions (Scottsdale, AZ, USA) [37]. This is a commercial device capable

of measuring the spatially resolved losses of an OF at 1310 nm down to a resolution of 50 cm with a pulse duration of 5 ns. These parameters were selected to obtain the best possible resolution for the measurements. The signal power at 1310 nm is rated at <1 mW. One should be careful not to let the total losses (which will cumulate over the irradiated distance) exceed the optical budget of the OTDR in use, that, for this setup, is around 10 dB.

### 2.3. Experimental Setup

To investigate the capability of this OF to perform distributed RIA measurements inside the IdeFIX X-ray machine (100 kV, W target) of the Laboratoire Hubert Curien (Saint Etienne, France) [38], we employed 26 m of ULL-PSCF, divided in sections, as shown in Figure 2. The combination of 2 m exposed (EF) and 5 m shielded (SF) sections of the fiber resulted in a non-uniform exposition to the X-ray beam, which could then be exploited to investigate the capacity of the sensor to provide spatially resolved radiation detection. The three EF sections were coiled in 3 concentric monolayer spirals, where EF1 was the innermost, and EF3 was the outermost. All the SF sections were completely covered by multiple 5 mm thick tungsten plates, allowing for stopping the X-rays before they reach the optical fiber.

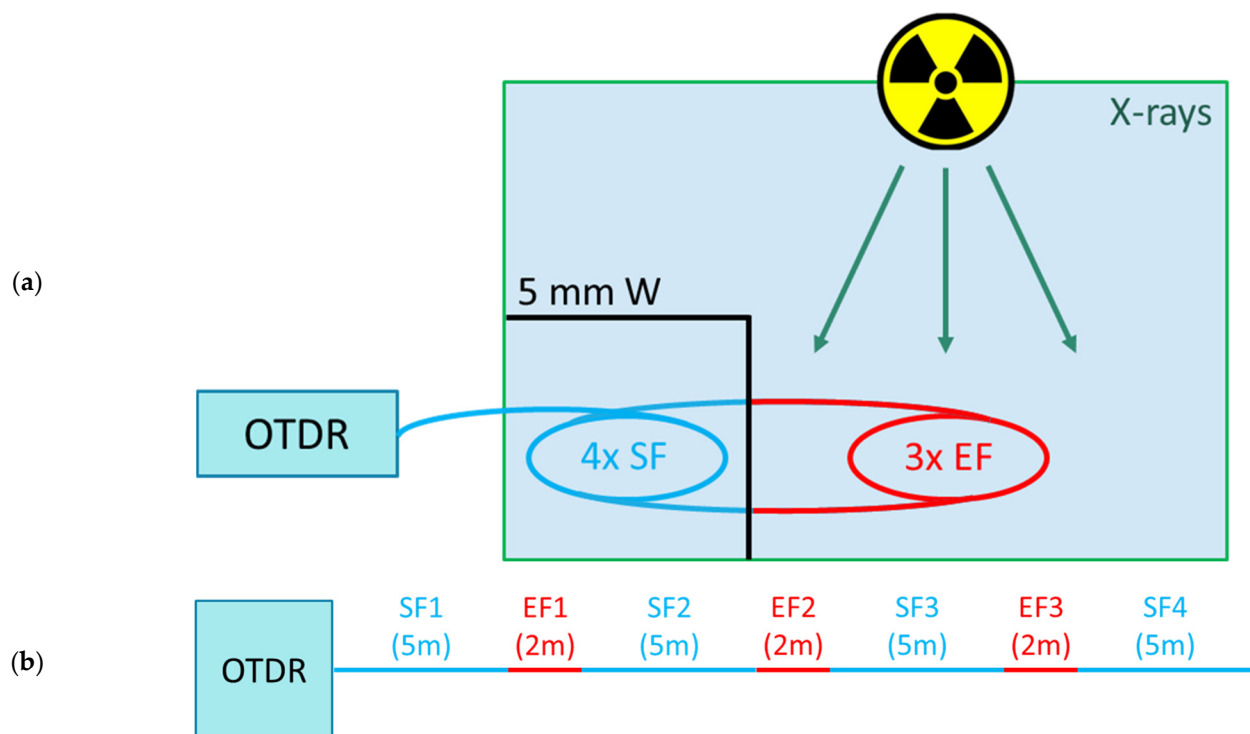


**Figure 2.** Schematics of the distributed RIA setup. (a) Disposition of the optical fibers inside the IdeFIX irradiator. The black lines represent the tungsten plates. (b) Distribution between shielded (SF) and exposed (EF) sections of the OF under test.

### 2.4. Irradiation Procedure

The ULL-PSCF response was investigated at room temperature using the stepped irradiation profile illustrated in Figure 3, the same used in [23]. The dose rate was varied only by adjusting the X-ray tube current, changing neither the distance between the tube and the sample under test nor the voltage of the tube. The irradiation sequence is composed of a cycle of 5 runs at increasing dose rates: 0.045, 0.28, 0.56, 5.6, and 16.8 Gy/s. Each run lasted 5 min, so the accumulated doses for each step were, respectively, 13.4, 84, 168, 1680, and 5080 Gy. Note that these doses exceed the values usually covered by RIA-based distributed dosimeters with P- or Al-doped fibers, limited to below 1 kGy. A 20 min recovery time is considered between two consecutive runs. Then, after 60 min of recovery,

the whole cycle is repeated but in reverse order. Finally, 5 expositions at the highest dose rate (16.8 Gy/s), each 5 min long and separated by 60 min of pause each time, were carried out. After this process ended, the fiber under test had been exposed to a total cumulated dose of ~39 kGy. The whole irradiation process was repeated for 7 iterations with a 2 h pause between runs, to investigate the evolution of the fiber RIA characteristics with the cumulated dose. The goal of this irradiation sequence is to evaluate the capability of this fiber to follow quick changes in the irradiation conditions and the possibility to implement it in a reusable radiation detector. It also permits distinguishing between the growth in permanent losses, observable between successive irradiation runs, and transient losses, present during irradiations.

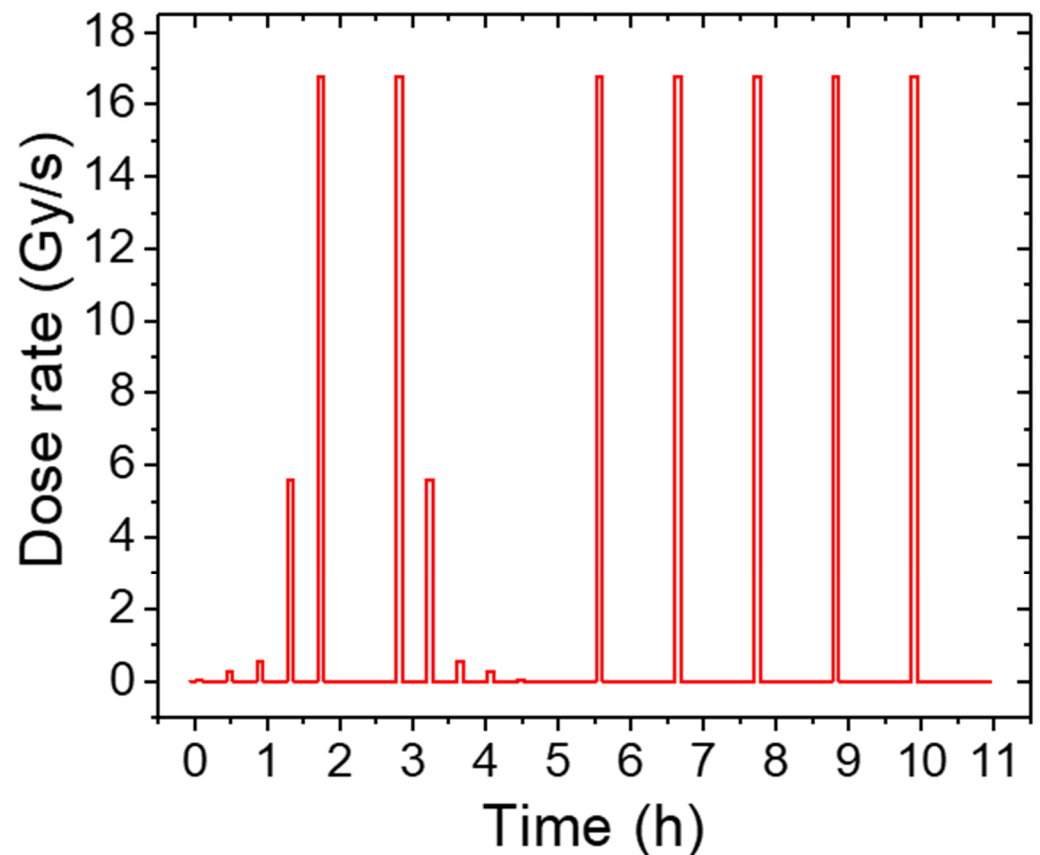


**Figure 3.** Irradiation sequence implemented for OF characterization with our X-ray machine. At each dose rate, the irradiation was maintained for 5 min, while the recovery between steps lasted 20 min for the first 5 steps, sweeping the dose rates; then 60 min before another cycle of 5 steps separated by 20 min pauses; and finally, 5 identical steps each separated by 60 min.

### 2.5. RIA Calculation from an OTDR Trace

RIA is defined as the increase in fiber losses when an OF is exposed to ionizing radiation. As such, it is estimated as the incremental losses after a certain dose per unit length. Starting from an OTDR trace, the RIA at different points of the fiber can be calculated as the difference of the negative slope of the OTDR trace during irradiation and the one acquired before irradiation, to correct for the intrinsic losses of the OF. In this paper, three methods are used to estimate the spatially resolved RIA: the derivative over distance of the OTDR traces, the estimation of the negative slope along the three EFs, and the difference in losses between the shielded areas before and after the exposed sections. A first classification among the three is that the second and third methods need the EF zones to be known a priori. The first method is then used in this work to search for the exposed sections of the fibers. The EFs can then be investigated better with the other two methods. The removal of



the intrinsic losses of the fiber was performed for all three methods and is not repeated in each explanation.

#### 2.5.1. First Method: Derivative over Distance of the OTDR Trace

With this method, the RIA can be calculated estimating the first order derivative along sections of the fiber. This method can be implemented to search the irradiated fiber sections, scanning the entire fiber length for radiation-induced losses. To correctly assess the RIA of a certain fiber section, the length of this section should not be shorter than the resolution of the OTDR, in this case 50 cm. This value is then the shortest length that is possible to investigate with this solution. If the irradiated section were to be shorter than 50 cm, it would not be possible to correctly assess the radiation-induced losses in that zone. In this work, a resolution of 50 cm was used to search for the 2 m long EFs.

#### 2.5.2. Second Method: Negative Slope

This method consists of performing a simpler linear regression fit on the exposed section of the optical fiber, which then needs to be known, and extracting the negative slope along this section. This can improve the precision of the RIA estimation, as there will be more points to work with for the slope estimation than in the first method. If the EF is longer than the OTDR spatial resolution, this method permits a better estimation of the RIA level.

#### 2.5.3. Third Method: SF Difference

The third method used to calculate the spatially resolved RIA from an OTDR trace can be only applied if the distribution of exposed sections along the fiber is known a priori. This method consists of subtracting the losses of the fiber sections before and after the irradiated section and dividing it by the length of the latter. As an example, to calculate the RIA along EF2, one would need to subtract the losses seen along SF3 from the losses of SF2. This method is limited by the spatial resolution of the trace along the shielded areas, instead of the exposed one, and can be affected by fluctuations happening in both the shielded areas. This method can then be more sensitive to fluctuations along the fiber, but it remains a very powerful tool in the case the EF is smaller than the resolution of the instrument.

### 3. Results and Discussions

#### 3.1. OTDR Trace

The raw result of an OTDR measurement is shown in Figure 4. Here, the black curve reports the complete trace, which includes the initial transport fiber and the reflected amplitude peak related to the interface at the end of the fiber under test (FUT). The blue curves show the four 5 m long shielded sections (SF) of the ULL-PSCF, while the red curve correspond to the three 2 m long sections that were exposed to the X-rays (EF). Figure 5 reports the OTDR trace of the 26 m ULL-PSCF when pristine (blue curve) and under irradiation at two dose rates (black and green). These traces were acquired during the sixth iteration, after the fiber had been irradiated to 196 kGy. This choice was made arbitrarily among the sixth iteration starting from the second one, after 39 kGy, as during the first iteration, the last points of EF3 and, consequently, SF4 fell outside the optical budget of the OTDR. The RIA effect is clearly visible in the three exposed sections (in orange in the figure), as the slope of the trace decreases monotonically with the dose rate, while the losses of the shielded sections remain flat.

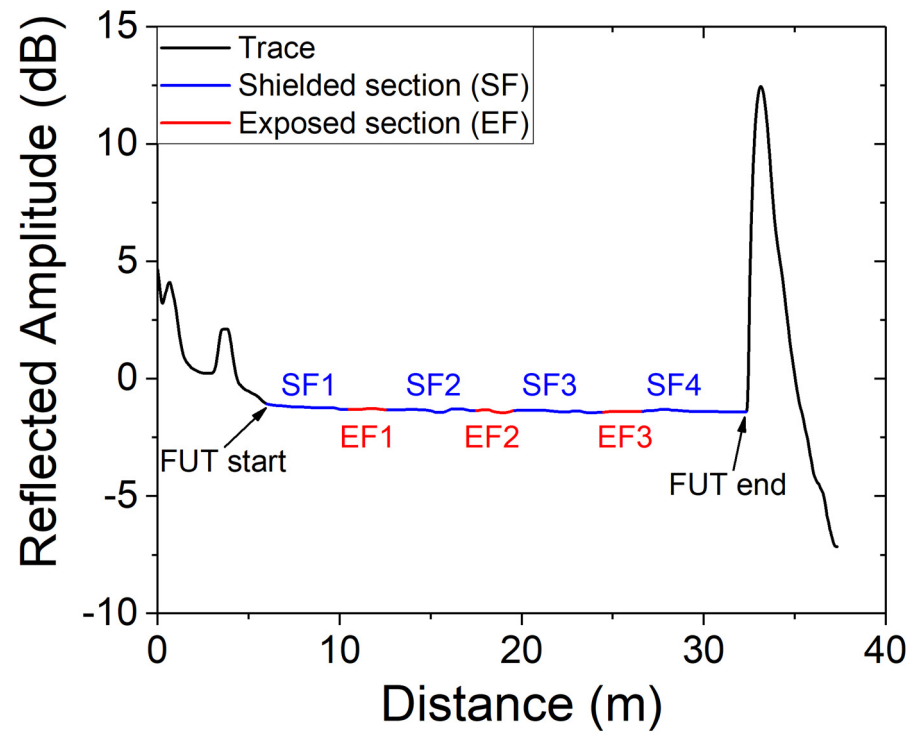


**Figure 4.** OTDR trace before irradiation. The black, blue, and red curves show the complete trace, the shielded sections of the FUT (SF), and the exposed sections of the FUT (EF), respectively.

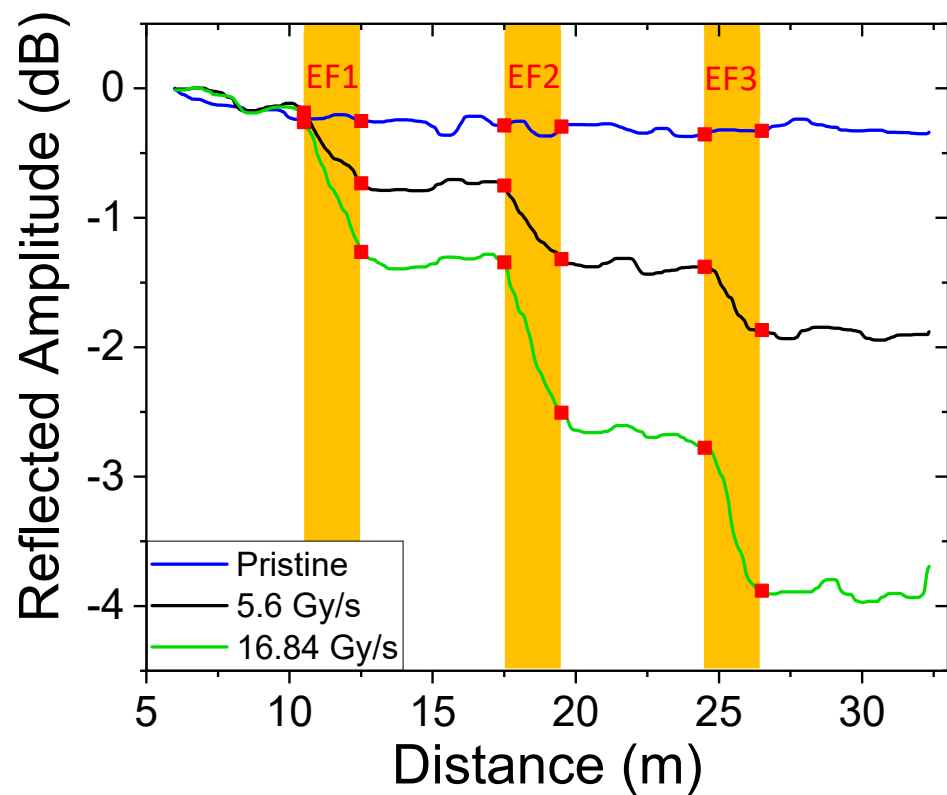


**Figure 5.** OTDR traces of the FUT only before (blue) and after a 5 min irradiation at 5.6 (black) and 16.84 (green) Gy/s. Before these traces were acquired, the OF had already been irradiated up to 196 kGy of cumulated dose, during the sixth iteration. The red squares correspond to the points between the sections shown in Figure 2. The three orange areas highlight the sections of the fiber exposed to the X-ray beam.



### 3.2. RIA Estimation: Trace Derivative

Figure 6 is obtained by estimating the first-order derivative along each 50 cm of the fiber and subtracting the reference contribution from before the irradiation start. The curves report three different 5 min irradiations at the three reported dose rates. The chosen resolution permits the recognition of the three different EFs (in orange) for the two highest dose rates.

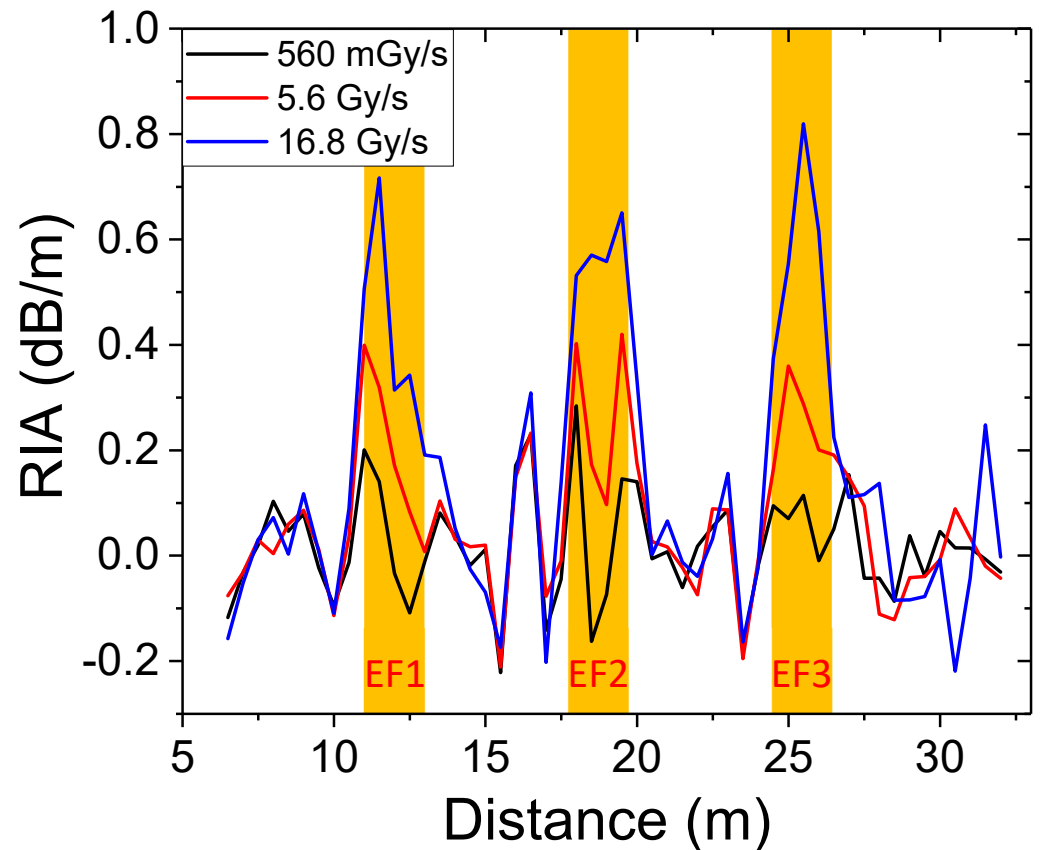


**Figure 6.** RIA over distance calculated as the negative slope of each 50 cm of fiber. The different curves report the results at the last point in a single 5 min irradiation at three different dose rates. The OTDR traces these curves originate from are inside the sixth irradiation iteration, after 196 kGy. The lower dose rates are not observable with this method.

As for the black curve at 560 mGy/s, the start of the irradiated sections can be recognized, but the fluctuations of the OTDR trace do not permit the recognition of the three EFs. At lower dose rates, the fluctuations are strong enough to completely mask the difference in losses between EFs and SFs.

### 3.3. RIA Kinetics

After having confirmed the positions of the three EFs along the optical fiber using the first method, it becomes possible to use the second and third methods to improve the RIA quantification. The RIA kinetics shown in Figure 7 were obtained evaluating the negative linear slope of the OTDR trace EF1 over time, the second method explained in Section 2.5.1. In Figure 7a, all seven iterations of the irradiation procedure explained in Section 2.4 are visible, together with the transient RIA peaks corresponding to the 5 min irradiations at different dose rates. Figure 7b,c highlight the responses obtained during the first and last irradiations of Figure 7a. With all these figures, the RIA behavior described in [23] can be recognized. During each irradiation, the transient losses quickly increase up to a maximum value and then decrease towards a lower one. The amplitude of these values clearly depends on the dose rate of each irradiation. The dose influence on this EF can first

be seen in the slight increase in the permanent losses after each irradiation. This increase is weaker than the one observed in [23], enough so that the fluctuations of the curves partly mask it. These oscillations are likely to be related to the combination of the uncertainties of the OTDR interrogator, of the RIA quantification procedure, and of temperature effects on the ULL-PSCF. This will need to be investigated in a future work.

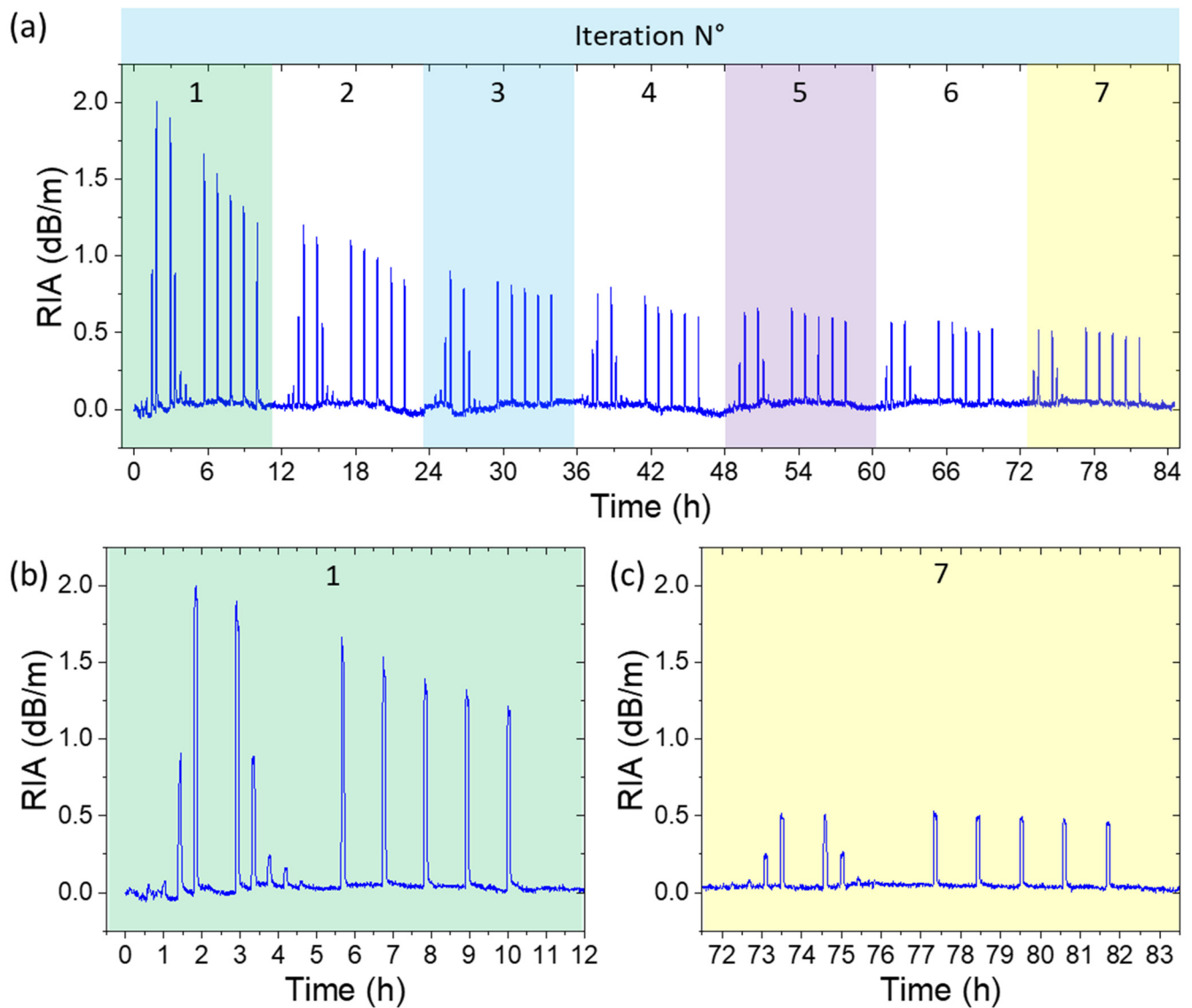


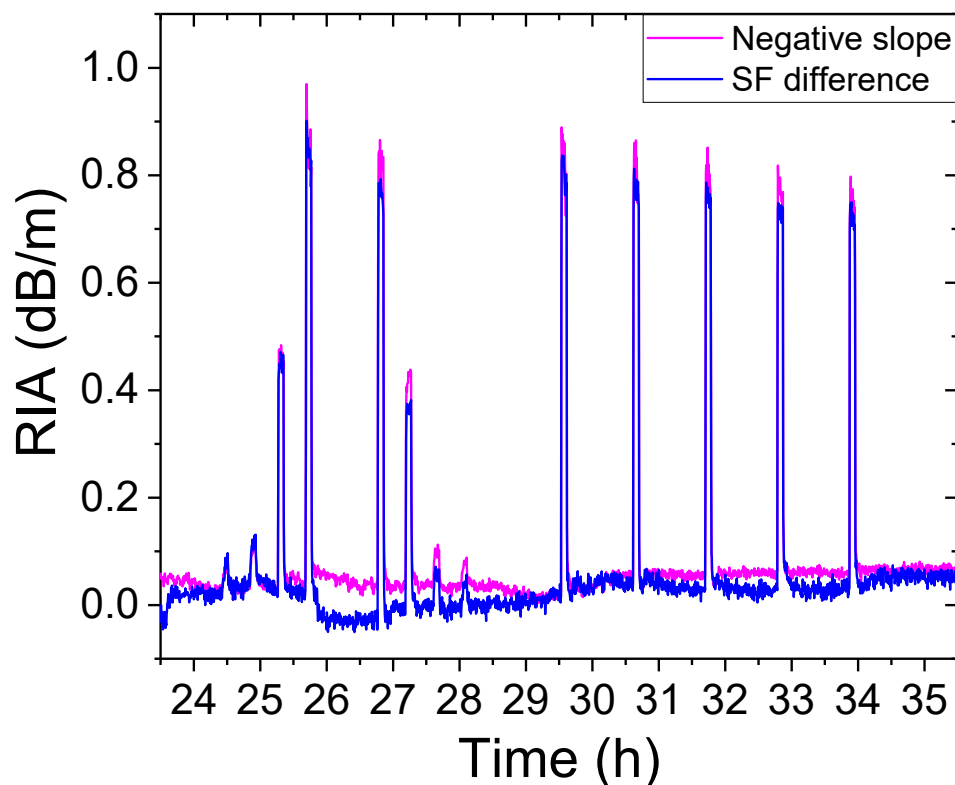
**Figure 7.** RIA kinetics of EF1. (a) Kinetics of the 7 iterations of the radiation procedure explained in Section 2.3. (b) Kinetics on the first repetition of the irradiation procedure. (c) Kinetics of the last repetition (after ~72 h) of the irradiation procedure. At this point, the exposed parts of the fiber have received around 235 kGy of dose.

The transient RIA contribution, during each irradiation, is also lower than that observed in previous work. The maximum RIA, observed through the first peak at maximum dose rate, (~2 dB/m) is six times lower than the observed amplitude in spectral measurements (~12 dB/m), as reported in Figure 1. This discussion is consistent with what was observed for this ULL-PSCF in [22], where the authors highlighted the strong influence of PB on the RIA of this OF. In this experiment, a more powerful source was used, in the order of 1 mW, compared to the white light source that was used for the spectral measurements taken in [23] (few  $\mu$ W). The effect of cumulative dose on these transient losses is a decrease in their amplitudes for the same dose rate—hence the sensitivity of the system as the dose

increases—together with a more ‘squared’ ON–OFF behavior, which is very appealing for a radiation detector. That was the idea at the base of the pre-irradiation in [23], but it was carried out only at 1 and 2 MGy, without any lower dose level. Thus, with the current study, it is possible to better estimate the minimum dose at which the response of the fiber can be considered stable. This can greatly help the preparation of these samples before their deployment, as the pre-treatment time will diminish. Indeed, from Figure 7c, it emerges that the transient losses appear now more quickly and stabilize faster to a fixed level. During the first irradiation procedure shown in Figure 7b, all the peaks corresponding to different dose rates are visible, down to the minimum dose rate of 45 mGy/s. As the height of the highest peaks decreases with dose, just like in [23], the system loses the capability to detect the lowest dose rates. At the seventh iteration, shown in Figure 7c, the minimum visible dose rate is 560 mGy/s. This reduction in sensitivity might rule out the usage of this fiber in lower dose rate applications, like space-related ones, but it can be compensated using more length. In the case where the more exposed zones of irradiation are known, a longer fiber can be coiled in these hot spots to improve the detection capabilities of the system. With longer EFs, the constraint of the resolution can also be relaxed. Thus, using longer pulses, hence larger resolutions, can improve the dynamics of the distributed detector.

### 3.3.1. RIA Kinetics: Methods Performance Comparison

As mentioned in Section 2.5, once the EF positions are known, there exist two methods to calculate the RIA along an exposed part of the fiber. The first is the estimation of the negative slope along the EF, reported in Figure 8 as ‘Negative slope’. The second is the difference between the average values of the SFs before and after an exposed part of the fiber, called ‘SF difference’ in Figure 8.



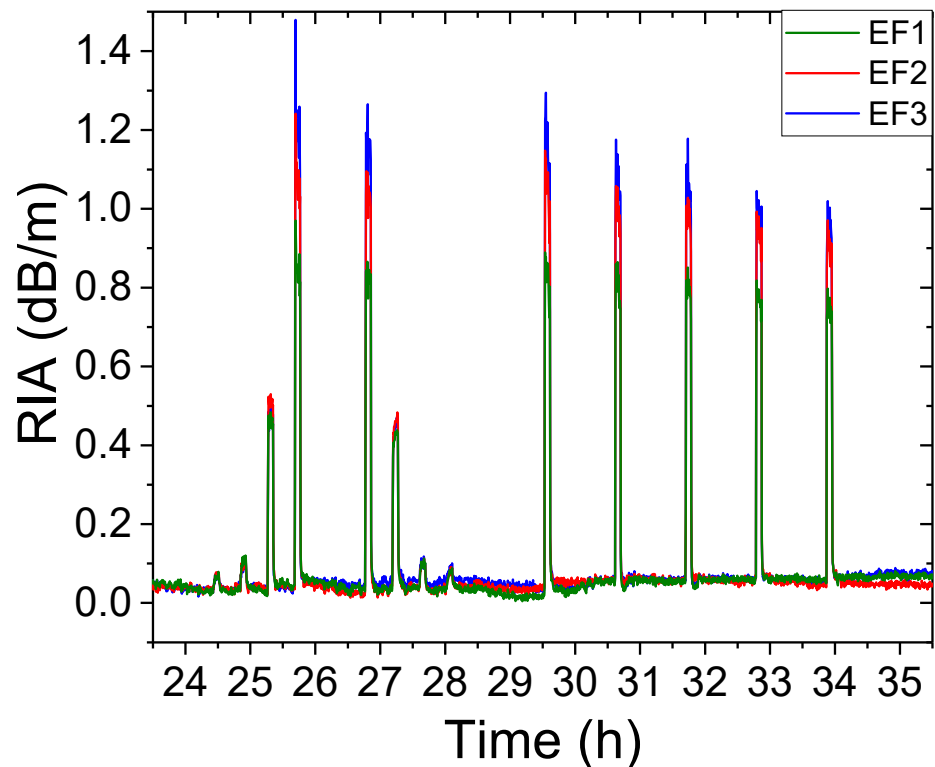
**Figure 8.** RIA kinetics of EF1 calculated with the two methods during the third iteration. The curve in blue was calculated as the negative slope along EF1 over time. The pink curve was obtained subtracting the average value of SF1 from the average value of SF2, divided by the length of EF1, 2 m.

Figure 8 shows the third iteration in the irradiation procedure. Before this cycle, the fiber received around 78 kGy. The differences in the two curves can be explained by the

different errors involved in the RIA estimation. The 'Negative slope' curve was calculated as the negative slope over time of EF1. As such, any fluctuation present in the OTDR trace along EF1 will affect the linear fit used to calculate the RIA. On the other hand, the blue curve was calculated as the difference between the average value across SF2 and the average value across SF1, all divided by the length of EF1, 2 m. This quantity is then influenced by the fluctuations in the two shielded areas. With our setup, the quality of the 'Negative slope' method seems to be more performant. One can see that the fluctuations of the permanent losses, when there was no irradiation, are smaller. This can be explained by the lowered sources of uncertainties in this first method. The estimation of the RIA in this method is performed along a single section of the fiber, whereas in the SF difference, the calculation is performed between two sections of the fiber. This means that the fluctuations along the two SFs both contribute to the measurement error. Even more, if they are not perfectly shielded, SFs can still be affected by a much weaker dose rate, which might influence the difference between them, and subsequently the RIA estimation. Still, this method remains very powerful in case the exposed length of the fiber is shorter than the resolution of the instrument. In this case, the difference between the SFs before and after the interested EF still permits the estimation of RIA, given that the radiation-induced losses are enough to surpass the noise level. An alternative solution could implement the use of radiation hard fibers for the SFs, and consequently improve the efficacy of the measurement by reducing the 'parasitic' RIA on these parts of the fiber. This introduces one figure of merit that can be used to choose between the two methods, the length of the fiber sections at play. The moment the irradiated area is very short, the SF difference method can permit precise RIA estimations even in case of a low number of points on the EF under study. On the other end, if the SFs are too short or outside the dynamic range of the OTDR (as was the case for the first two irradiation cycles on EF3), one should implement the 'negative slope' method, as it will always be possible to implement it along any EF longer than 50 cm. All the rest of the RIA estimation in this work is then estimated with the 'negative slope' method.

### 3.3.2. RIA Kinetics: Exposed Zones Comparison

Figure 9 reports the RIA kinetics calculated across the three EFs as their respective negative slopes. As for Figure 8, at the beginning of these kinetics, the fiber had received around 78 kGy, making it the third iteration of the irradiation process. From this figure emerges that there exists a difference between the three EFs. More in detail, the RIA of EF3, the furthest away from the source, is higher than the RIA of EF2, which is in turn higher than EF1's. This phenomenon is again explained by the high sensitivity to PB of this fiber, as the RIA induced inside the first EF reduces the amount of light travelling inside EF2. As such, the annealing of defect centers absorbing along EF2 is less pronounced, which results in a higher RIA along this section. The same effect is then present between EF2 and EF3, where the RIA of EF2 reduces the amount of light seen by EF3, resulting in an even higher transient RIA under the same irradiation condition. This phenomenon can be a weak point in the possibility of using this setup for dose rate sensing, as it introduces a dependence of the RIA on the distance between the investigated zone and the detector. In the measurements reported in this paper, this phenomenon seems to be relevant only at the highest dose rate, 16.8 Gy/s, where the EF2 is 48% higher than EF1 during the first iteration. As for EF3, as stated before, its RIA went outside the optical budget of the OTDR during the first iteration, so it is not possible to compare its level to EF1's. In the second iteration, the RIA of EF3 was 63% higher than EF1's, and 23% higher than EF2's. At 5.6 Gy/s, the difference was significant only during the first iteration, where EF2 was 20% higher than EF1, and EF3 was 37% higher than EF1. At all the other doses, the difference between the three EFs at all dose rates is less than 10% and does not always increase monotonically with the distance from the detector. This difference between EFs decreases with dose, like the amount of RIA for a same dose rate.



**Figure 9.** RIA kinetics comparison between the three exposed sections of the fiber for the third repetition of the irradiation process. At this point, the fiber had received around 78 kGy of dose.

At the seventh iteration, EF2 and EF3 are only 1% higher than EF1, with no visible difference between EF2 and EF3. From this experiment alone, it is not possible to estimate if this decrease in PB efficacy is only due to the lower RIA levels involved, hence lower injected intensity differences between the three EFs, or if the defects responsible for the transient RIA after a certain dose are stable enough to be less affected by the PB. It seems anyway that the effect of PB distributed along the fiber seems to be strong enough only at very high dose rates, leaving room for a possible implementation of this setup as a distributed dose rate sensor.

### 3.4. Dose Rate Distributed Sensor Calibration

The radiation response of this OF and its compatibility with OTDR techniques show great promise for spatially distributed radiation detection applications, as seen in the previous sections. To further evaluate the possibilities of this technology, the RIA vs. dose rate response at multiple pre-irradiation levels needs to be addressed, so as to investigate the possibility of using this combination as a single-ended distributed dose rate sensor. The effect of PB explained in Section 3.3.2 is of concern only at the highest dose rate, 16.8 Gy/s. The difference between the three EFs at the four lower dose rates is always less than 10%, with the exception of the first iteration between EF2 and EF3. These dose rates can then be investigated for a possible calibration of the RIA over dose rate characteristic at different doses for this ULL-PSCF. Furthermore, the transient RIA behavior of this ULL-PSCF stabilizes with cumulated dose, both in terms of ON–OFF response, saturation of permanent losses, and decrease in the sensitivity to PB of the complete system. The cumulated dose is then introduced as a figure of merit that can define the profile of use of this OF. On one side, a non-irradiated OF has very high sensitivity to dose rate, a very welcome feature for a radiation sensor. This comes though with low repeatability and high sensitivity to PB, which will make it difficult to quantify the dose rate reliably. On the other hand, a higher cumulated dose permits to sacrifice some of the fiber sensitivity for a more reliable measurement. Figure 10 shows the transient RIA over dose rate response of

averaged across the three EFs for different pre-irradiation doses. The transient contribution was quantified by averaging the last three minutes of each irradiation and subtracting the three minutes just before the same irradiation, to remove the contribution of the permanent losses. The RIA vs. dose rate response is monotonic at all doses. The points at low dose rates are clearly influenced by the fluctuations in the constant losses observed in Figure 8.

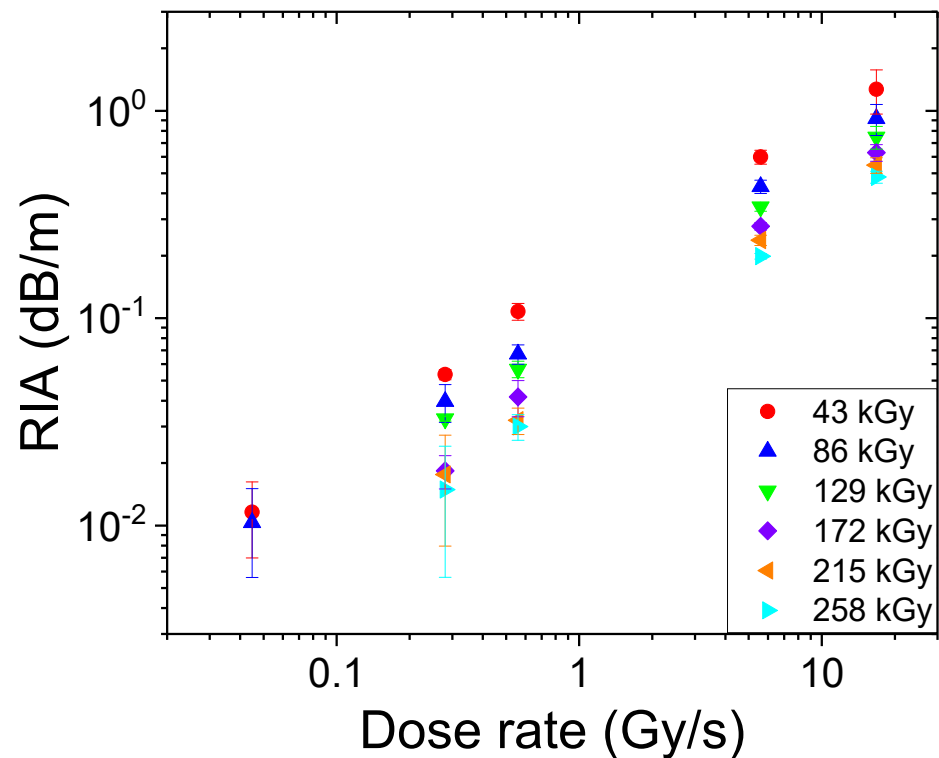


**Figure 10.** Transient RIA over dose rate at different pre-irradiation doses averaged across the three EFs. These values are calculated as the average across the last 3 min of irradiation minus the average of the 3 min before each irradiation starts. The error bands show the standard deviation across the three EFs.

The investigated doses do not seem to be enough to obtain the RIA vs. dose rate linearity of this OF, as the dose dependence is still important. This effect is lower and lower as the pre-irradiation dose increases and, with the results in [23], it is expected to become less important at higher doses. The results then suggest that the investigated doses are still not enough to permit an RIA vs. dose rate calibration of the fiber.

#### 4. Conclusions

This paper showed the promise of combining a radiation-sensitive ULL-PSCF and an OTDR to obtain a single-ended distributed radiation monitor. Furthermore, when combined with the results discussed in [23], the information presented in this work point towards the feasibility of building a radiation detector capable of working at very high doses, thanks to its capability to ‘self-reset’ after irradiation. One important parameter to be optimized is the length of the exposed sections of the fiber. Longer EFs can improve the sensitivity of the system, then permitting the detection of lower dose rates, and permit more precise measurements. In this case, users would still need to be careful about the possible running out of optical budget of the interrogation instrument, which would cause the furthestmost parts of the fibers to no be visible by the instrument. Interestingly enough, compared to concurrent solutions, namely, point detectors, this would simply shorten the maximum distance that could be monitored with this OF. Indeed, as the RIA of this OF ‘resets’ after irradiation, returning to a very low permanent level, this problem will



not persist. As for the possibility of evolving this solution into a distributed dose rate sensor, the system is showing promise. As was observed at MGy levels, increasing the pre-irradiation dose reduces the sensitivity of the transient RIA against dose rate. The RIA vs. dose rate will need to be investigated at higher doses, as the response over the investigated values is still not linear. One concern is the thermal response of the fiber, as the stability of the defects that contribute to the permanent and transient RIA could change with temperature. New studies will need to be devoted to the study of this fiber's response and to the possible implementation of more advanced interrogation techniques, e.g., optical frequency domain reflectometry.

**Author Contributions:** Conceptualization, L.W., A.M. and S.G.; Data curation, L.W.; Formal analysis, L.W.; Funding acquisition, S.G.; Investigation, L.W., A.M. and S.G.; Methodology, L.W.; Project administration, S.G.; Resources, A.M., Y.O., E.M., A.B. and S.G.; Software, L.W.; Supervision, A.M. and S.G.; Validation, A.M., Y.O., E.M., A.B. and S.G.; Visualization, L.W., A.M. and S.G.; Writing—original draft, L.W.; Writing—review and editing, A.M., Y.O., E.M., A.B. and S.G. All authors have read and agreed to the published version of the manuscript.

**Funding:** The results presented in this paper were obtained within the framework of the EU project RADNEXT, receiving funding from the European Union's Horizon 2020 research and innovation program, grant agreement no. 101008126.

**Data Availability Statement:** The data presented in this study are available on reasonable request from the corresponding authors.

**Conflicts of Interest:** The authors declare no conflicts of interest.

## References

1. Di Francesca, D.; Brugger, M.; Vecchi, G.L.; Girard, S.; Morana, A.; Reghioua, I.; Alessi, A.; Hoehr, C.; Robin, T.; Kadi, Y. Qualification and Calibration of Single-Mode Phosphosilicate Optical Fiber for Dosimetry at CERN. *J. Light. Technol.* **2019**, *37*, 4643–4649. [[CrossRef](#)]
2. Meyer, A.; Morana, A.; Weninger, L.; Balcon, N.; Melin, G.; Mekki, J.; Robin, T.; Champavère, A.; Saigné, F.; Boch, J.; et al. Toward an Embedded and Distributed Optical Fiber-Based Dosimeter for Space Applications. *IEEE Trans. Nucl. Sci.* **2023**, *70*, 583–589. [[CrossRef](#)]
3. Di Francesca, D.; Toccafondo, I.; Li Vecchi, G.; Calderini, S.; Girard, S.; Alessi, A.; Ferraro, R.; Danzeca, S.; Kadi, Y.; Brugger, M. Distributed Optical Fiber Radiation Sensing in the Proton Synchrotron Booster at CERN. *IEEE Trans. Nucl. Sci.* **2018**, *65*, 1639–1644. [[CrossRef](#)]
4. Toccafondo, I.; Marin, Y.E.; Guillermain, E.; Kuhnenn, J.; Mekki, J.; Brugger, M.; Pasquale, F.D. Distributed Optical Fiber Radiation Sensing in a Mixed-Field Radiation Environment at CERN. *J. Light. Technol.* **2017**, *35*, 3303–3310. [[CrossRef](#)]
5. Henschel, H.; Körfer, M.; Kuhnenn, J.; Weinand, U.; Wulf, F. Fibre Optic Radiation Sensor Systems for Particle Accelerators. *Nucl. Instrum. Methods Phys. Res. Sect. A Accel. Spectrometers Detect. Assoc. Equip.* **2004**, *526*, 537–550. [[CrossRef](#)]
6. Imamura, K.; Suzuki, T.; Gozen, T.; Tanaka, H.; Okamoto, S. *Application of Nd<sup>3+</sup>-Doped Silica Fibers to Radiation Sensing Devices*; Gillespie, C.H., Greenwell, R.A., Eds.; SPIE: Orlando, FL, USA, 1987; p. 62. [[CrossRef](#)]
7. Anderson, D.R.; Johnson, L.; Bell, F.G. Early Developments. In *Troubleshooting Optical Fiber Networks*; Elsevier: Amsterdam, The Netherlands, 2004; pp. 1–12, ISBN 978-0-12-058661-5.
8. Healey, P. Instrumentation Principles for Optical Time Domain Reflectometry. *J. Phys. E Sci. Instrum.* **1986**, *19*, 334–341. [[CrossRef](#)]
9. Hartog, A.H. *An Introduction to Distributed Optical Fibre Sensors*, 1st ed.; CRC Press: Boca Raton, FL, USA, 2017; ISBN 978-1-315-11901-4.
10. Girard, S.; Kuhnenn, J.; Gusarov, A.; Brichard, B.; Van Uffelen, M.; Ouerdane, Y.; Boukenter, A.; Marcandella, C. Radiation Effects on Silica-Based Optical Fibers: Recent Advances and Future Challenges. *IEEE Trans. Nucl. Sci.* **2013**, *60*, 2015–2036. [[CrossRef](#)]
11. Griscom, D.L. Radiation Effects on Glass. In *Encyclopedia of Materials Science and Engineering*; Pergamon Press Ltd.: Oxford, UK, 1986; Volume 6.
12. Girard, S.; Alessi, A.; Richard, N.; Martin-Samos, L.; De Michele, V.; Giacomazzi, L.; Agnello, S.; Francesca, D.D.; Morana, A.; Winkler, B.; et al. Overview of Radiation Induced Point Defects in Silica-Based Optical Fibers. *Rev. Phys.* **2019**, *4*, 100032. [[CrossRef](#)]
13. Griscom, D.L. Optical Properties and Structure of Defects in Silica Glass. *J. Ceram. Soc. Jpn.* **1991**, *99*, 923–942. [[CrossRef](#)]
14. Griscom, D.L. *Nature of Defects and Defect Generation in Optical Glasses*; Levy, P.W., Ed.; SPIE: Albuquerque, NM, USA, 1985; p. 38. [[CrossRef](#)]
15. Griscom, D.L.; Friebele, E.J.; Long, K.J.; Fleming, J.W. Fundamental Defect Centers in Glass: Electron Spin Resonance and Optical Absorption Studies of Irradiated Phosphorus-doped Silica Glass and Optical Fibers. *J. Appl. Phys.* **1983**, *54*, 3743–3762. [[CrossRef](#)]

16. Tomashuk, A.L.; Grekov, M.V.; Vasiliev, S.A.; Svetukhin, V.V. Fiber-Optic Dosimeter Based on Radiation-Induced Attenuation in P-Doped Fiber: Suppression of Post-Irradiation Fading by Using Two Working Wavelengths in Visible Range. *Opt. Express* **2014**, *22*, 16778. [CrossRef] [PubMed]
17. Weninger, L.; Campanella, C.; Morana, A.; Fricano, F.; Marin, E.; Ouerdane, Y.; Boukenter, A.; Alia, R.G.; Girard, S. Calibration in the Visible and Infrared Domains of Multimode Phosphosilicate Optical Fibers for Dosimetry Applications. *IEEE Trans. Nucl. Sci.* **2023**, *70*, 1908–1916. [CrossRef]
18. Li Vecchi, G.; Di Francesca, D.; Kadi, Y.; Ricci, D.; Brugger, M.; Campanella, C.; Alessi, A.; Ouerdane, Y.; Girard, S. In-Situ Regeneration of P-Doped Optical Fiber Dosimeter. *Opt. Lett.* **2020**, *45*, 5201. [CrossRef] [PubMed]
19. Morana, A.; Campanella, C.; Vidalot, J.; De Michele, V.; Marin, E.; Reghioua, I.; Boukenter, A.; Ouerdane, Y.; Paillet, P.; Girard, S. Extreme Radiation Sensitivity of Ultra-Low Loss Pure-Silica-Core Optical Fibers at Low Dose Levels and Infrared Wavelengths. *Sensors* **2020**, *20*, 7254. [CrossRef] [PubMed]
20. De Michele, V.; Marcandella, C.; Morana, A.; Campanella, C.; Vidalot, J.; Paillet, P.; Gaillardin, M.; Marin, E.; Ouerdane, Y.; Boukenter, A.; et al. Pulsed X-ray Radiation Response of Ultralow Loss Pure-Silica-Core Optical Fibers. *Phys. Status Solidi A* **2022**, *219*, 2100519. [CrossRef]
21. Girard, S.; Morana, A.; De Michele, V.; Campanella, C.; Vidalot, J.; Marin, E.; Boukenter, A.; Paillet, P.; Ouerdane, Y. Radiation Responses of Ultra-Low Loss Pure-Silica-Core Optical Fibers in the Visible to Infrared Domains. *Opt. Mater. X* **2022**, *16*, 100191. [CrossRef]
22. Campanella, C.; Morana, A.; De Michele, V.; Vidalot, J.; Marin, E.; Boukenter, A.; Ouerdane, Y.; Paillet, P.; Girard, S. Photobleaching Effect on the Radiation-Induced Attenuation of an Ultralow Loss Optical Fiber at Telecommunication Wavelengths. *Phys. Status Solidi A* **2022**, *219*, 2100518. [CrossRef]
23. Weninger, L.; Morana, A.; Campanella, C.; Vidalot, J.; Marin, E.; Ouerdane, Y.; Boukenter, A.; Alia, R.G.; Girard, S. Radiation Monitoring with Radiosensitive Pure-Silica Core Ultra-Low Loss Optical Fiber. *IEEE Trans. Nucl. Sci.* **2024**. [CrossRef]
24. Kashaykin, P.F.; Tomashuk, A.L.; Vasiliev, S.A.; Ignatyev, A.D.; Shaimerdenov, A.A.; Ponkratov, Y.V.; Kulsartov, T.V.; Kenzhin, Y.A.; Gizatulin, S.K.; Zholdybayev, T.K.; et al. Radiation Resistance of Single-Mode Optical Fibres with View to in-Reactor Applications. *Nucl. Mater. Energy* **2021**, *27*, 100981. [CrossRef]
25. Tomashuk, A.L.; Golant, K.M. *Radiation-Resistant and Radiation-Sensitive Silica Optical Fibers*; Dianov, E.M., Ed.; SPIE: Moscow, Russia, 2000; p. 188. [CrossRef]
26. Tamura, Y.; Sakuma, H.; Morita, K.; Suzuki, M.; Yamamoto, Y.; Shimada, K.; Honma, Y.; Sohma, K.; Fujii, T.; Hasegawa, T. The First 0.14-dB/Km Loss Optical Fiber and Its Impact on Submarine Transmission. *J. Light. Technol.* **2018**, *36*, 44–49. [CrossRef]
27. Griscom, D.L. Self-Trapped Holes in Pure-Silica Glass: A History of Their Discovery and Characterization and an Example of Their Critical Significance to Industry. *J. Non-Cryst. Solids* **2006**, *352*, 2601–2617. [CrossRef]
28. Martinet, C.; Martinez, V.; Coussa, C.; Champagnon, B.; Tomozawa, M. Radial Distribution of the Fictive Temperature in Pure Silica Optical Fibers by Micro-Raman Spectroscopy. *J. Appl. Phys.* **2008**, *103*, 083506. [CrossRef]
29. Wang, R.P.; Tai, N.; Saito, K.; Ikushima, A.J. Fluorine-Doping Concentration and Fictive Temperature Dependence of Self-Trapped Holes in SiO<sub>2</sub> Glasses. *J. Appl. Phys.* **2005**, *98*, 023701. [CrossRef]
30. Yamaguchi, M.; Saito, K.; Ikushima, A.J. Fictive-Temperature-Dependence of Photoinduced Self-Trapped Holes in a—SiO<sub>2</sub>. *Phys. Rev. B* **2003**, *68*, 153204. [CrossRef]
31. Lines, M.E. Can the Minimum Attenuation of Fused Silica Be Significantly Reduced by Small Compositional Variations? I. Alkali Metal Dopants. *J. Non-Cryst. Solids* **1994**, *171*, 209–218. [CrossRef]
32. Agrawal, G.P. *Fiber-Optic Communication Systems*, 5th ed.; Wiley: Hoboken, NJ, USA, 2021; ISBN 978-1-119-73736-0.
33. Vedda, A.; Chiodini, N.; Di Martino, D.; Fasoli, M.; Keffer, S.; Lauria, A.; Martini, M.; Moretti, F.; Spinolo, G.; Nikl, M.; et al. Ce<sup>3+</sup>-Doped Fibers for Remote Radiation Dosimetry. *Appl. Phys. Lett.* **2004**, *85*, 6356–6358. [CrossRef]
34. Mones, E.; Veronese, I.; Vedda, A.; Loi, G.; Fasoli, M.; Moretti, F.; Chiodini, N.; Cannillo, B.; Brambilla, M. Ce-Doped Optical Fibre as Radioluminescent Dosimeter in Radiotherapy. *Radiat. Meas.* **2008**, *43*, 888–892. [CrossRef]
35. Faustov, A.V.; Gusarov, A.V.; Mégret, P.; Wuilpart, M.; Zhukov, A.V.; Novikov, S.G.; Svetukhin, V.V.; Fotiadi, A.A. Application of Phosphate Doped Fibers for OFDR Dosimetry. *Results Phys.* **2016**, *6*, 86–87. [CrossRef]
36. Corning, N. 14831 Corning Vascade Optical Fibers. Available online: [http://www.tlc.unipr.it/cucinotta/cfa/datasheet\\_Vascade.pdf](http://www.tlc.unipr.it/cucinotta/cfa/datasheet_Vascade.pdf) (accessed on 24 March 2024).
37. VIAVI MTS-4000 V2. Available online: <https://www.viavisolutions.com/fr-fr/produits/plateforme-mts-4000-v2#overview> (accessed on 16 March 2024).
38. Meyer, A.; Lambert, D.; Morana, A.; Paillet, P.; Boukenter, A.; Girard, S. Simulation and Optimization of Optical Fiber Irradiation with X-Rays at Different Energies. *Radiation* **2023**, *3*, 58–74. [CrossRef]

**Disclaimer/Publisher’s Note:** The statements, opinions and data contained in all publications are solely those of the individual author(s) and contributor(s) and not of MDPI and/or the editor(s). MDPI and/or the editor(s) disclaim responsibility for any injury to people or property resulting from any ideas, methods, instructions or products referred to in the content.